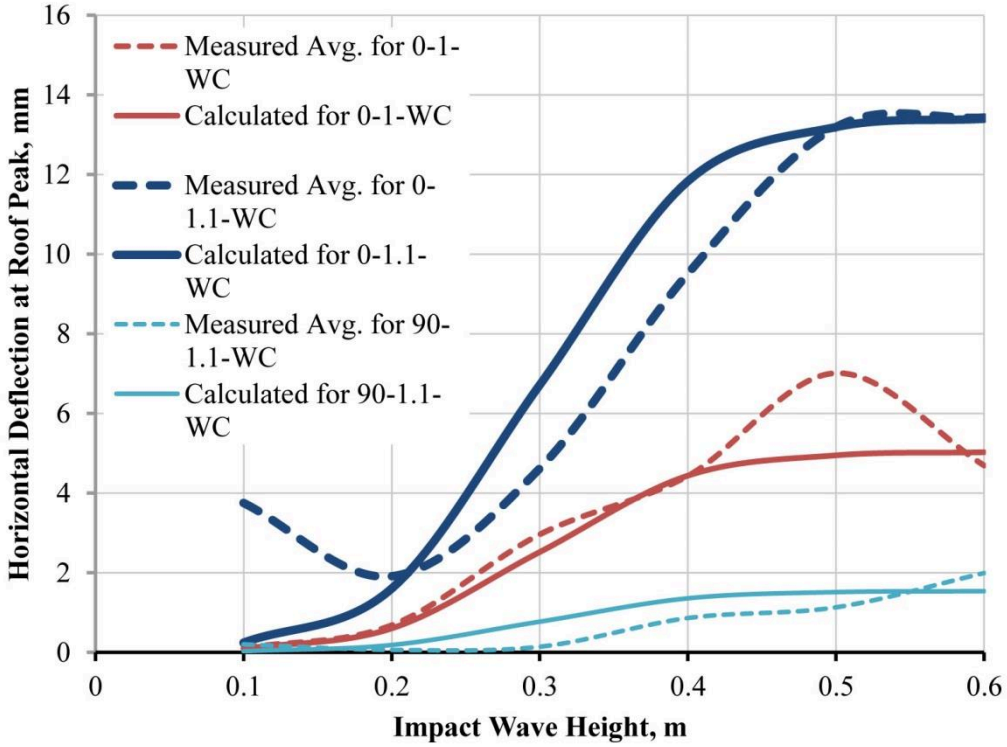

Figure 3. Modeled and measured deflections for various configurations.

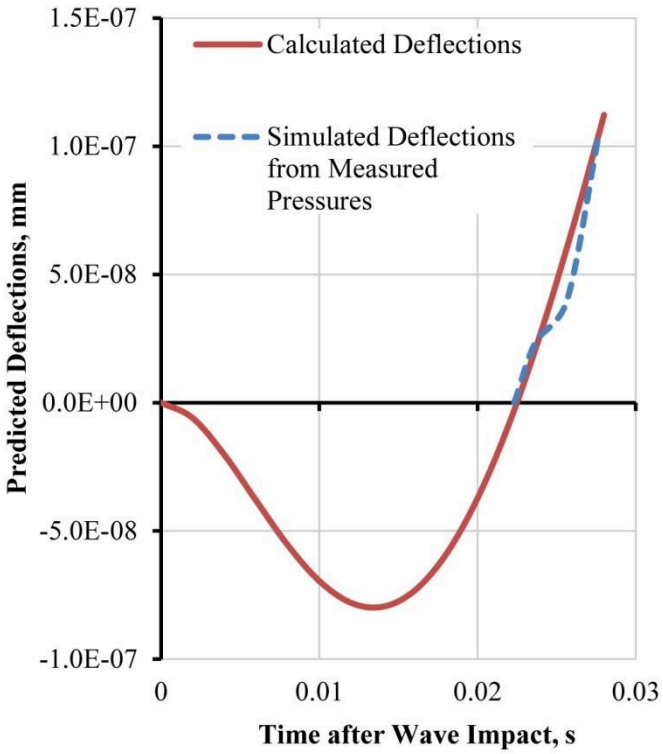

Figure 4. Predicted deflections for wave impact on tank plate wall.

The predicted response is similar to what negative is observed in closed hydraulic systems created by fluid transients, commonly referred to as water hammer. There appears to be

significant potential to reduce impact pressures on wave impacted structures by inclusion of components similar to those designed to mitigate pressure transients. It may be possible to dampen initial negative deflections such that the positive deflection will also be reduced by changing the system's natural frequency, as occurred with reduced ullage pressure in the Lugni et al. study (2010).

Normalized equations closely predict maximum deflections for various wave heights with an undefined peak k_g value. In order to consider whether the normalized equations are applicable beyond the scale model residential structure studied by OSU, equations were applied to measured pressure curves from wave impacts on a tank plate wall in the Lugni et al. study (2010). As shown in Figure 4, the predictive equation produces a good curve fit for measured data in the referenced study assuming a t_c value of 0.0225 (frequency 11.11 Hz) and peak k_g value of π.

CONCLUSIONS

Normalized equations provide a basis for research and opportunity to further develop equations for predicting peak forces and deflections on structures from wave impacts. Close correlation to seismic structural responses encourages further investigation to potentially expand predictive methods for wave impacts by applying seismic design theory.

The intent of this brief study was to evaluate the consistent time delay in measured deflection response from wave impacts. Time to peak deflection appears to be largely a function of the impacted structure's natural frequency. Negative pressure and/or no deflection observed in the initial time period before positive deflections occur are predicted and directly proportional to peak deflections in magnitude.

Coastal structures can be designed with systems that either dampen the response to hydraulic transients or change the impacted system's natural frequency to reduce resultant wave loads. If equations are refined and validated through additional research, consideration of seismic-type design analysis, load dampening, and seismic type connections may become a matter of course for coastal structures.

WORKS CITED

ASCE (American Society of Civil Engineers). (2014) *Minimum Design Loads for Buildings and Other Structures,* Standard ASCE/SEI 7-10. Third printing. ASCE, Reston, VA.

FEMA (Federal Emergency Management Agency). (1999) *FIA-TB-9, Design and Construction Guidance for Breakaway Walls Below Elevated Coastal Buildings.*

FEMA Mitigation Assessment Team. (2006) "Report on Hurricane Katrina in the Gulf Coast," JFO Briefings Presentation, 99.

FEMA. (2011) *P-55, Coastal Construction Manual Principles and Practices of Planning, Siting, Designing, Constructing, and Maintaining Residential Buildings in Coastal Areas.* Fourth Edition. Volumes I, II & CCM Resources Manual.

FEMA. (2009) *P-550, Recommended Residential Construction for Coastal Areas Building on Strong and Safe Foundations.* Second Edition.

Filiatrault, A, I. Christovasilis, A. Wanitkorkul, and J.W. van de Lindt. (2010). "Experimental Seismic Response of a Full-Scale Light-Frame Wood Building", *ASCE Journal of Structural Engineering,* 136(3), 246-254.

Hattori, M., A. Arami, T. Yui. (1994) "Wave impact pressure on vertical walls under breaking waves of various types," *Coastal Engineering* (22)1-2, 79-114.

Lugni, C., M. Miozzi, and M. Brocchini. (2010) "Evolution of the air cavity during a wave impact," http://www.dipmat.univpm.it/aimeta2009/Atti%20Congresso/MECCANICA_FLUIDI/lugni_paper213.pdf.

Miles, J. (2007). "Surge impact loading on wood residential structures," Proceedings of the 2007 Earthquake Engineering Symposium for Young Researchers. http://mceer.buffalo.edu/education/reu/2007/content/27Miles.pdf.

Sutoyo, D. (2009). "Hysteretic characteristics of wood-frame structures under seismic motions," Dissertation (Ph.D.), CIT, http://resolver.caltech.edU/CaltechETD:etd-05172009-153304.

van de Lindt, J.W., R. Gupta, R. Garcia, and J. Wilson. (2009). "Tsunami Bore Forces on a Compliant Residential Building Model." *Engineering Structures,* 31, 2534-2539.

van de Lindt, J.W., A. Graettinger, R. Gupta, T. Skaggs, S. Pryor, and K. Fridley. (2007). "Performance of Woodframe Structures During Hurricane Katrina." *ASCE Journal of Performance of Constructed Facilities*; 21(2), 108-116.

White, K.B.D., T. H. Miller, R. Gupta. (2009). "Seismic performance testing of partially and fully anchored wood-frame shear walls," *Wood and Fiber Science,* 41(4), 396-413.

Wilson, J.S., R. Gupta, J.W. van de Lindt, M. Clauson, and R. Garcia. (2009)."Behavior of a One-Sixth Scale, Wood-Framed Residential Structure Under Wave Loading." *ASCE Journal of Performance of Constructed Facilities,* 23 (5), 336-345.

Wilson, J.S., R. Gupta, J.W. van de Lindt, and D.T. Cox. (2010). "Behavior of Wood-Framed Residential Structure Under Surge Wave Loading." 11th World Conference on Wood Engineering, Trentino, Italy, June 2010.

Wu, N.T., H. Oumeraci, H. W. Partenscky (1994). "Numerical Modelling of Breaking Wave Impacts on a Vertical Wall," *Coastal Engineering,* 1672-1686.

Lateral Restraining Stiffness Effects on the Bridge Deck-Wave Interaction under Hurricane Waves

Guoji Xu, Ph.D.[1] and C. S. Cai, Ph.D., P.E., F.ASCE[2]

[1]Research Assistant, Center for Computation & Technology, Louisiana State Univ., Baton Rouge, 70803; Former Student, Dept. of Civil and Environmental Engineering, Louisiana State Univ., Baton Rouge, LA 70803. E-mail: gxu2@lsu.edu
[2]Edwin B. and Norma S. McNeil Distinguished Professor, Dept. of Civil and Environmental Engineering, Louisiana State Univ., Baton Rouge, LA 70803 (corresponding author). E-mail: cscai@lsu.edu

ABSTRACT

An investigation of the lateral restraining stiffness effect on the bridge deck-wave interaction under hurricane waves is conducted numerically using a dynamic mesh updating technique. At first, a mass-spring-damper system is implemented in a commercial CFD program in order to realize that the bridge superstructure can vibrate laterally under the wave actions. Then, a wave model based on the Stokes 2nd order wave theory is developed and verified with analytical solutions. The shear stress transport (SST) k-ω model is used as the turbulence closure for the RANS equations. This developed methodology is further verified with experimental measurements in the literature which assures its valid applications in the following parametric study. Finally, general characteristics of the structural vibration and the wave forces are observed and discussed through a parametric study. The obtained results show that increasing the structural flexibilities in the lateral/transverse direction does not necessarily benefit the bridge structure with an obvious force reduction for both the horizontal and vertical forces on the bridge superstructure.

Key words: Bridge deck-wave interaction; Coastal bridges; Wave forces; Computational fluid dynamics (CFD); Dynamic mesh updating technique; Hurricane waves.

INTRODUCTION

The combination of the storm surge and high waves induced by hurricanes during the last decade destroyed many coastal low-lying bridges along the Gulf of Mexico in the United States (Graumann et al. 2005; Robertson et al. 2007; Okeil and Cai 2008; Padgett et al. 2008). These post-disaster reports conclude that submerged bridge decks during a coastal inundation are subjected to huge hydrodynamic wave loads and the existing short- and medium-span coastal bridges are rarely designed for this type of wave forces. To reveal the failure mechanisms of the damaged bridges and to propose potential guidelines for better designing or retrofitting coastal bridges under such extreme natural events, many experimental and numerical studies have been conducted (AASHTO 2008; Sheppard and Marin 2009; Xiao et al. 2010; Jin and Meng 2011; Bradner et al. 2011; Bozorgnia and Lee 2012). However, most of these studies focus on the rigid setups that the bridge model is fixed in the wave flume/tank experimentally and computationally. Very few studies investigated the dynamic characteristics (flexible setups) of the bridge deck-wave interaction (Bradner et al. 2011; Xu and Cai 2015). Fig. 1 shows a schematic diagram for the bridge deck-wave interaction under hurricane induced waves, where the structural self-stiffness (consist of the substructure stiffness and the interface stiffness) plays a significant role

in the dynamic analysis.

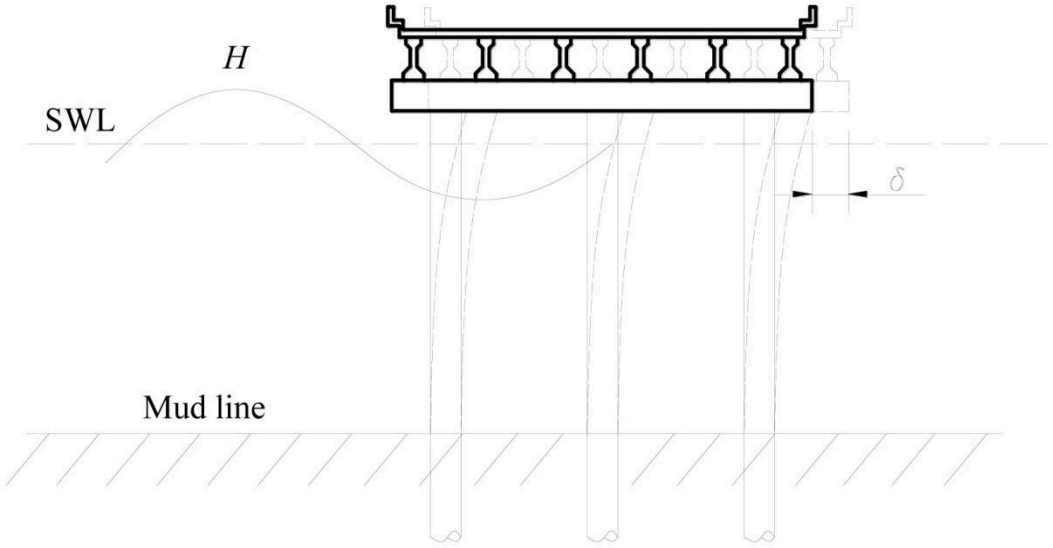

Fig. 1 Schematic diagram for the bridge deck-wave interaction under hurricane induced waves. *H* refers to the wave height; *δ* is the structural displacement for the bridge deck; SWL refers to the still water level; Mud line refers to where the piles can be deemed as rigided supported. The interface is not plotted for convenient purpose.

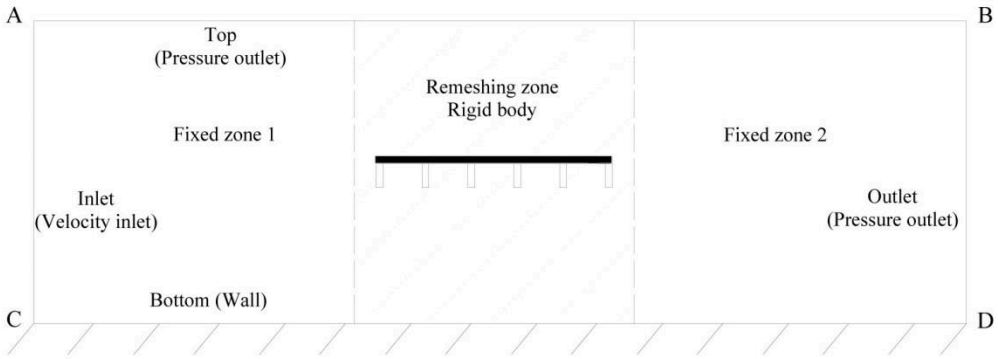

(a) Remeshing zone and Fixed zone in the computational domain

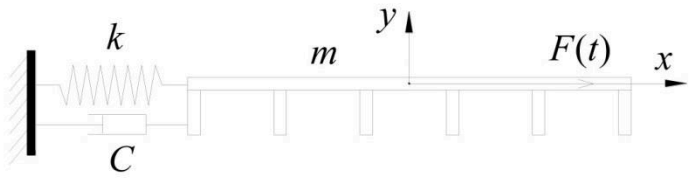

(b) The mass-spring-damper system

Fig. 2 Schematic diagram of the computational domain for the mass-spring-damper system. In this system, *m* is the unit length weight of the bridge deck, *k* is the lateral restraining stiffness, and *c* is the damping coefficient.

The dynamic analysis for the bridge deck-wave interaction problems is an emerging topic, but it is of significant importance. On the one hand, the bridge deck would have unneglected vibrations under certain waves (Bradner et al. 2011). Bradner et al. (2011) developed a flexible setup using the springs, which can be adjusted according to a finite element analysis of the whole

bridge structure, installed between the specimen and the end anchorage block on the walls of the wave flume. However, limited data were reported but some general observations. On the other hand, similar to the mitigation ideas used in the earthquake engineering, base isolations, cable restraints, shear keys, and shape memory alloys maybe employed to adjust the structural stiffness in order to reduce the damage to structures (Okei and Cai 2008). This is based on the assumption that a larger lateral displacement of the bridge deck along the wave propagation would dissipate more wave energy. As such, a systematic study regarding to the bridge deck-wave interaction under hurricane induced waves is needed, which is essential for designing and retrofitting coastal bridges that would experience hurricane events in their service period.

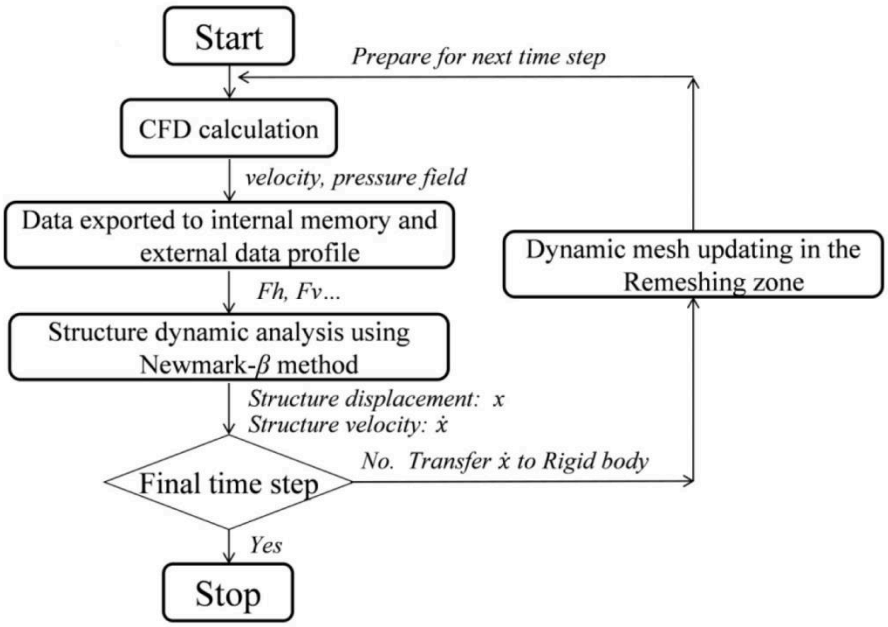

Fig. 3 Flow chart for the bridge deck-wave interaction using the proposed mass-spring-damper system

The objective of the present study is to investigate the lateral restraining stiffness effects on the bridge deck-wave interaction under hurricane waves (Stokes 2nd order wave model is adopted as a representative) in order to provide an in-depth view of the bridge deck performance with different flexible setups. At first, a mass-spring-damper system representing the SDOF system is implemented in a commercial CFD program (Fluent, Academic Version, V15.0) to realize the bridge deck vibrations under wave conditions. Then, a wave model based on the Stokes 2nd order wave theory is developed and verified with the analytical solutions and experimental measurements. Finally, a parametric study is conducted in order to obtain the general characteristics of the structural vibrations and the wave forces on the bridge deck.

NUMERICAL METHODOLOGY AND EXPERIMENTAL VERIFICATION

The Mass-Spring-Damper System

The bridge deck model considering the dynamic features can be deemed as a mass-spring-damper system in order to accommodate the SDOF system, as shown in Fig. 2. The whole computational domain is partitioned into three parts, two fixed zones and one remeshing zone. The mesh in the fixed zones (zones 1 and 2) remains the same as its original mesh. The mass-

spring-damper system is incorporated in the remeshing zone and their combination is treated as a rigid body, which will move laterally in both directions using the layering mesh method. For the setup of the layering mesh method, the height based method is chosen with the split factor 0.4 and the collapse factor 0.2.

For the boundary conditions in the computational domain, the line AB is pressure outlet, keeping the pressure in the air phase the same as the operating pressure (101, 325 Pa); the line AC is velocity inlet; the bottom line CD is modeled with a no slip stationary wall condition; and the line BD is set as the pressure outlet. The water phase in the computational domain for prescribed wave conditions will be patched through Fluent at the initialization stage. The sketch of the geometry of a typical coastal bridge deck model is also shown in Fig. 2. This prototype bridge, which will be used in the parametric study, consisting of a slab and six AASHTO type III girders, is designed to carry two traffic lanes on the deck and can be commonly found connecting coastal communities (Huang and Xiao 2009; Xiao et al. 2010). The width of the superstructure is 10.45 m, the girder height is 1.05 m, and the slab depth is 0.3 m. All the six girders, each with a width of 0.3 m, are simplified as rectangles and evenly distributed.

The vibration of the rigid body (the bridge deck) in the *x*/lateral direction can be described as the following equations:

$$\ddot{x} + 2\xi\omega_0\dot{x} + \omega_0^2 x = (t)/m \tag{1}$$

$$k = m\omega_0^2 \tag{2}$$

$$\omega_0 = \frac{2\pi}{T_s} \tag{3}$$

$$c = 2\xi\omega_0 m \tag{4}$$

where x is the instantaneous displacement of the bridge model in the x direction, ξ is the damping ratio, ω_0 is the natural frequency of the bridge superstructure, $F(t)$ is the instantaneous horizontal force integrated from the hydraulic pressure along the bridge model surface, and T_s is the structural vibration period. Therefore, based on known mass, vibration period, and the damping ratio of the bridge structure, the corresponding lateral restraining stiffness and the damping coefficient can be calculated.

The procedure for simulating the bridge deck-wave interaction using the layering mesh method, one dynamic mesh updating technique, is demonstrated in Fig. 3. The velocity and pressure filed are firstly obtained through the CFD calculation in each time step. The horizontal force $F(t)$, the vertical force, and the moment can then be obtained real-timely by the user defined function (UDF) macros of Compute_Force_And_Moment and exported to corresponding files. Subsequently, structural dynamic analysis is conducted using the *Newmark-β* method by substituting the horizontal force $F(t)$ obtained at the current time step into equation (1). The displacement and velocity of the bridge deck can thus be achieved. Finally, this velocity is attributed to the rigid body by the macros of DEFINE_CG_MOTION. The bridge deck will correspondingly move to a new position followed by the dynamic mesh updating in the remeshing zone. Once the mesh is updated, the whole computational domain is ready for the next time step and this loop will continue to the final time step (Xu and Cai 2015; Xu et al. 2015).

Wave Generation and Verification

To capture the turbulent features for the bridge deck-wave interaction, the shear stress transport (SST) k-ω model is used as the turbulence closure for the RANS equations. The reason

is that this turbulent model has its advantages over the *k-ε* model, one common turbulence model, such that both the flow field with a high Reynold number and the near wall field with a relatively low Reynold number can be more appropriately computed. The equations for the SST *k-ω* model are given as follows:

$$\frac{\partial}{\partial t}(\rho k)+\frac{\partial}{\partial x_i}(\rho k u_i)=\frac{\partial}{\partial x_j}\left(\Gamma_k \frac{\partial k}{\partial x_j}\right)+G_k-Y_k+S_k \tag{5}$$

$$\frac{\partial}{\partial t}(\rho \omega)+\frac{\partial}{\partial x_j}(\rho \omega u_j)=\frac{\partial}{\partial x_j}\left(\Gamma_\omega \frac{\partial \omega}{\partial x_j}\right)+G_\omega-Y_\omega+S_\omega \tag{6}$$

where k is turbulent kinetic energy which determines the energy in the turbulence, ω is the specific dissipation which determines the scale of the turbulence; Γ_k and Γ_ω are the effective diffusivity of k and ω; G_k represents the generation of turbulence kinetic energy due to the mean velocity gradients, calculated from G_k; G_ω is the generation of ω; Y_k and Y_ω are the dissipation of k and ω, respectively; D_ω, is the cross-diffusion term; and S_k and S_ω, are user-defined source terms.

In the present study, Stokes 2nd order wave theory is employed to represent one typical wave type induced by hurricanes. In the simulations, water is assumed as an incompressible, viscous fluid and the Volume of Fluid (VOF) method is utilized to track the dynamic free surface. For the setups of the SST *k-ω* model in Fluent, the pressure-based solver (segregated) is chosen for the transient flow and the Pressure-Implicit with Splitting of Operators (PISO) scheme is utilized for the pressure-velocity coupling method. Further details of the numerical setups can be found in Xu and Cai (2015).

A numerical flume with the size of 40 m in length and 2.5 m in height is chosen (in order to accomadate the experimental study by Bradner et al. (2011)) for the verification of the wave profiles with analytical results. A wave height of 0.5 m is demonstrated here. Based on the mesh sensitivity study by Xu and Cai (2015), the grid resolutions are: dx = 0.02m, 0.01m, and 0.04m are for the near velocity inlet zone, main computational zone, and far field from the main computational zone, respectively; dy = 0.04m, 0.01m and 0.02m for the air zone, the near water zone, and the deep water zone, respectively. The time step is 0.005 s. The comparison of the wave profiles between the numerical simulations and the analytical results is shown in Fig. 4, which shows a good agreement.

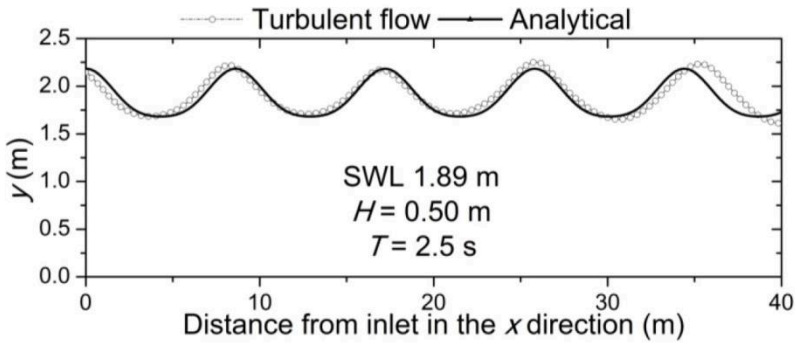

Fig. 4 Comparisons of the free surface profiles

Verification of the Mass-Spring-Damper System

The verification of the mass-spring-damper system is carried out against the experimental

study by Bradner et al. (2011), where a 1:5 scaled bridge deck model was considered. The width of the bridge deck model is 1.94 m, the girder height is 0.23 m, and the deck depth is 0.05 m. In the present study, the girder is simplified as a rectangle and its width is 0.06 m. There are 6 girders in total and the railing effect is not considered. The grid meshes are the same as used in the verification with the analytical results and fine meshes are adopted near the walls of the bridge deck model, as shown in Fig. 5 (Xu and Cai 2015). Detailed information about the flexible setups of the soft springs and medium springs can be found in Bradner et al. (2011).

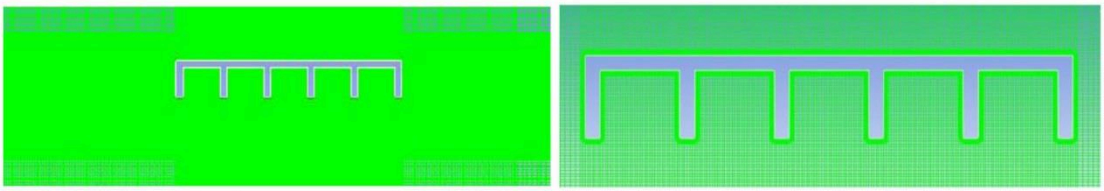

(a) Grid mesh in the computational domain (b) Grid mesh nearby the bridge model

Fig. 5 Grid mesh for the computational domain and near the bridge model

Comparisons of the wave forces between the flexible setups and the rigid setup when H = 0.50 m are shown in Fig. 6. It is observed that: (a) while much smaller negative horizontal forces are found for the rigid setup, significant negative horizontal forces are observed for the flexible setups, especially the soft springs setup; (b) a phase lag can be observed between the positive peak horizontal forces of the rigid setup and the flexible setups; and (c) there is no significant difference on the positive peak vertical forces. These observations are in good agreement with the experimental study by Bradner et al. (2011), which ensures a valid prediction of the bridge deck-wave interaction process.

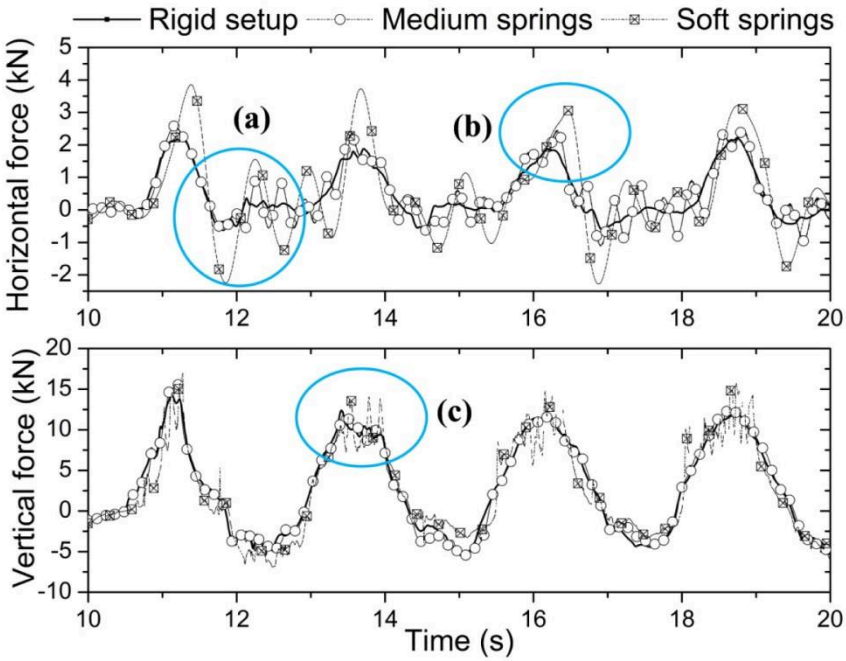

Fig. 6 Comparisons of wave forces when H = 0.50 m

PARAMETRIC STUDY

In the parametric study, six sets of stiffness corresponding to six vibration periods and a

damping coefficient ξ of 0.05 are chosen based on the study by Bradner et al. (2011), as shown in Table. 1. In the simulations, the mass is taken as 9716 kg per unit length according to the study by Xiao et al. (2010) (154000 kg/15.85 m=9716 kg per unit length).

Table 1 Parameters for the mass-spring-damper system

Cases	T (s)	m (kg)	ξ	k (N/m)	c (Ns^2/m)
k1813	0.46	9716	0.05	1812724	13271
k998	0.62	9716	0.05	997847	9846
k630	0.78	9716	0.05	630461	7827
k425	0.95	9716	0.05	425011	6426
k170	1.5	9716	0.05	170477	4070
k96	2.0	9716	0.05	95893	3052

The wave height is 2.0 m, the water depth is 8.4 m, and the wave period is 5.5 s (Chen et al. 2009). The computational domain is 10 m high and 200 m long. The geometry of the bridge deck model is shown in Fig. 2. Six different structure elevations are considered to simulate in field conditions, as listed in Table 2, where C_S ($C_S = S/H_b$) is the coefficient of submersion depth and is negative when the bottom of the superstructure is under the SWL; S = the distance from the bottom of the bridge superstructure to the SWL; and H_b = superstructure depth. The momentum center is the moment center due to the vertical force and horizontal force, and it is located at the middle height of the deck for each case. The abbreviation name of each case is designated according to both the bridge elevation (the value refers to the elevation of the bottom of the girder) and the submersion coefficient; for example, E8.4/CS(0) stands for the case when the bottom of the bridge model is 8.4 m from the sea bed and the corresponding coefficient of submersion depth C_S is 0.

Table 2 Structure elevations and corresponding coefficients

Cases	Bridge elevation (Bottom of the girder) (m)	S(m)	$C_S = S/H_b$	Momentum Center	
				x (m)	y (m)
E9.0/CS(0.444)	9.0	0.6	0.444	95.225	10.2
E8.7/CS(0.222)	8.7	0.3	0.222	95.225	9.9
E8.4/CS(0)	8.4	0	0	95.225	9.6
E8.1/CS(-0.222)	8.1	-0.3	-0.222	95.225	9.3
E7.8/CS(-0.444)	7.8	-0.6	-0.444	95.225	9.0
E7.5/CS(-0.667)	7.5	-0.9	-0.667	95.225	8.7

Structural vibration

One example of the bridge deck displacement is shown in Fig. 7 where the case of E7.8/CS(-0.444) with different restraining stiffnesses starts from the original position, 95.225 m, when the simulation begins. The vibration amplitude of Case k96 is relatively larger than those of other cases with higher stiffnesses. The maximum bridge deck displacements for all the six structure elevations with different restraining stiffnesses are shown in Fig. 8. The displacement values (in the landward direction) show the same trends, namely, the less restraining stiffness, the larger the deck displacement. For a given stiffness of all the six cases, the deck displacement differs from each other, which are also related to the values of the horizontal forces.